View Article Online
View Journal

Dalton Transactions

An international journal of inorganic chemistry

Accepted Manuscript

This article can be cited before page numbers have been issued, to do this please use: H. V. Le, M. Babak, M. A. Ehsan, M. Altaf , L. Reichert, A. Gushchin, W. H. Ang and A. Isab, *Dalton Trans.*, 2020, DOI: 10.1039/D0DT01411G.

ROYAL SOCIETY OF CHEMISTRY

rsc.li/dalton

View Article Online
DOI: 10.1039/D0DT01411G

ARTICLE

Highly cytotoxic gold(I)-phosphane dithiocarbamate complexes trigger an ER stress-dependent immune response in ovarian cancer cells

Received 00th January 20xx,
Accepted 00th January 20xx

DOI: 10.1039/x0xx00000x

Hai Van Le,[a, ≠] Maria V. Babak,[a, ≠] Muhammad Ali Ehsan,[b] Muhammad Altaf,[b, c] Lisa Reichert,[a] Artem L. Gushchin,[d, e] Wee Han Ang,*[a, f] Anvarhusein A. Isab*[g]

Ovarian cancer is a highly aggressive disease which is treated by surgery and platinum chemotherapy. However, a significant proportion of treated patients develop resistance to platinum treatment resulting in tumor relapse. Acquired platinum resistance has been recently correlated with activation of pro-survival endoplasmic reticulum (ER) stress responses. We hypothesized that Au complexes that induce severe ER stress might counteract pro-survival cellular attempts leading to the ER stress-mediated apoptosis and reduced platinum resistance. In this work, we prepared a series of highly cytotoxic Au^{I}-dialkyldithiocarbamate complexes and investigated their anticancer potential in ovarian cancer cells. Complexes demonstrated surprisingly low stability in chloroform, resulting in the formation of an Au chain polymer, which also displayed excellent cytotoxicity. Lead complex **2** induced oxidative stress and ER stress-mediated p53-independent apoptosis associated with PARP cleavage and cell cycle arrest at G_2/M phase. Importantly, **2** caused the surface exposure of calreticulin (CRT), which is the first step in the activation of cellular immunogenic response.

Introduction

Ovarian cancer is the fifth leading cause of cancer-related deaths in women. The standard treatment plans for a newly diagnosed disease include cytoreductive surgery and platinum-based chemotherapy including cisplatin (cDDP) and carboplatin; hence, the prognosis for women is defined by the stage of their malignancy and its sensitivity to platinum drugs.[1] Acquired platinum resistance in ovarian cancer was recently linked to the activated pro-survival cellular responses, including ER stress and autophagy.[2] Moreover, the overexpression of pro-survival ER stress markers correlated with poor survival of high-grade ovarian cancer patients.[3] ER stress in cancer cells occurs when the normal protein homeostasis is altered upon external or internal triggers, such as hypoxia or nutrient deprivation.[4, 5] Consequently, cancer cells activate an adaptive mechanism called unfolded protein response (UPR) to enhance protein folding and clearance of defective proteins.[6] However, when the duration or intensity of ER stress exceeds pro-survival capacity of cancer cells, they activate cell death mechanisms.[7] Therefore, chemotherapeutic agents capable of severe ER stress induction might lead to the suppression of cellular pro-survival responses, leading to the reduced drug resistance in ovarian cancer cells and improved treatment outcomes.

Organometallic Au complexes represent a promising alternative to cDDP for the treatment of resistant ovarian cancer, since they were demonstrated to induce ER stress-mediated apoptosis in a range of cancer cell lines.[8-10] Various Au^{I} and Au^{III} complexes demonstrate excellent anticancer potential, including Au^{I}-phosphane anti-rheumatoid arthritis drug, auranofin.[11-13] Auranofin induces oxidative and ER stress[8] and is currently undergoing Phase II clinical trials for the treatment of metastatic ovarian cancers.[14] Herein, we designed a series of highly potent Au(I)-phosphane dialkyldithiocarbamates and investigated their anticancer potential in ovarian cDDP-sensitive and cDDP-resistant cell lines in comparison with auranofin and cDDP. The dithiocarbamate moiety was chosen due to the well-known anticancer properties of Au^{I} and Au^{III} dithiocarbamate complexes and their potency against cDDP-resistant cell lines,[15-18] while [1,1′-biphenyl]-2-yldi-*tert*-butylphosphane moiety increased their lipophilicity. In addition, phosphane fragments are commonly incorporated into Au^{I} frameworks, leading to highly cytotoxic organometallics.[19, 20] In agreement with the design, Au^{I} complexes demonstrated high intracellular accumulation in ovarian cancer cells and the ability

[a] *Department of Chemistry, National University of Singapore,3 Science Drive 2, 117543 Singapore, E-mail: chmawh@nus.edu.sg*
[b] *Center of Research Excellence in Nanotechnology, King Fahd University of Petroleum & Minerals, Dhahran 31261, Saudi Arabia*
[c] *Department of Chemistry, Government College University Lahore, 54000 Lahore, Pakistan*
[d] *Nikolaev Institute of Inorganic Chemistry, Siberian Branch of Russian Academy of Sciences, 3 Acad. Lavrentiev Avenue, Novosibirsk 630090, Russia*
[e] *Novosibirsk State University, 2 Pirogov Street, 630090 Novosibirsk, Russia*
[f] *NUS Graduate School for Integrative Sciences and Engineering, Singapore*
[g] *Department of Chemistry, King Fahd University of Petroleum and Minerals, Dhahran 31261, Saudi Arabia, E-mail: aisab@kfupm.edu.sa*
[≠] Both authors contributed equally to this manuscript. ORCID: Maria V. Babak 0000-0002-2009-7837, Lisa Reichert 0000-0002-4684-8483, Artem L. Gushchin 0000-0003-3214-143, Wee Han Ang 0000-0003-2027-356X
Electronic Supplementary Information (ESI) available: NMR, HR-MS and IR spectra of **1**-**4,** crystallographic data for **1**, **2′**, **3** and **4**, concentration-effect curves and cell cycle analysis data. See DOI: 10.1039/x0xx00000x

to induce severe ER stress, resulting in the low nanomolar potency of novel compounds. Additionally, Au^{I} complexes showed the induction of ER stress-mediated CRT exposure, a known trigger for immune system response.

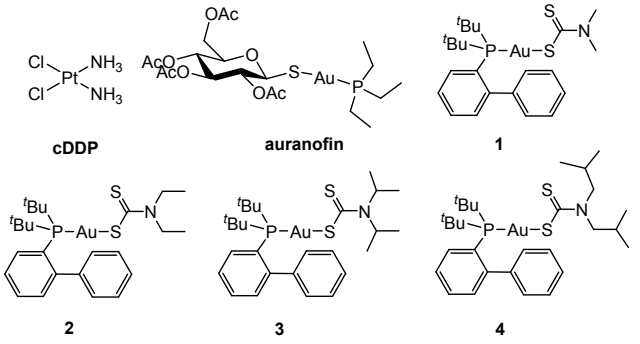

Scheme 1 Molecular structures of cDDP, auranofin and Au^{I}-phosphane complexes investigated in the current work.

Results and Discussion

Synthesis and characterization

A series of Au^{I}-phosphane dialkyldithiocarbamates **1**-**4** were prepared in good yields via metathesis reaction of the chloro[1,1'-biphenyl-2-yl)di-*tert*-butylphosphine] Au(I) complex and the respective sodium dialkyldithiocarbamate [Na(S_2CNR_2)] in MeOH/pyridine solutions. The addition of pyridine was essential to ensure the solubilization of the reaction mixture. The traces of pyridine were removed by crystallization of the complexes using hexane. The structures of **1**-**4** are presented in Scheme 1.

Novel complexes **1**-**4** were unambiguously characterized by ^{1}H and ^{31}P NMR spectroscopy (Fig. S1-S6), IR spectroscopy and mass spectrometry (Fig. S7-S10) and their purity was confirmed by elemental analysis and high resolution mass spectrometry. Complexes **1**-**4** are poorly soluble in H_2O, MeOH and DMSO and well-soluble in CH_2Cl_2, $CHCl_3$ and pyridine. All ^{1}H NMR spectra displayed six characteristic signals in the aromatic region (7.1-7.9 ppm) and two singlet signals in the aliphatic region (≈1.4 ppm), corresponding to a diphenyl and *tert*-butyl moieties of the phosphane ligand, respectively. FTIR spectra of **1-4** exhibited characteristic well-resolved and sharp bands (Fig. S11), in particular at 1476–1507 cm^{-1} region, which corresponds to the stretching vibration of N–CSS "thioureide" group. The presence of a split band at 940–1060 cm^{-1} indicated the unsymmetrical coordination through one of the sulphur atoms i.e. monodentate nature of dithiocarbamate moiety. Additionally, the coordination of phosphine and dithiocarbamate groups to the Au^{I} center was confirmed by the presence of ν(Au-P) and ν(Au-S) bands in the range of 272–289 and 195–202 cm^{-1}, respectively.

The ^{1}H NMR spectra of **1**-**4** were recorded in a variety of solvents, including pyridine-d^5, MeOH-d^4, DMSO-d^6 and $CDCl_3$. Due to poor solubility in DMSO, the ^{1}H NMR spectra of **2** and **4** in DMSO-d^6 could only be recorded after pre-heating of the solution and were of poor quality (Fig. S3 and S6). However, the signals remained unchanged for 10-14 d, indicating significant stability of these complexes in DMSO. Surprisingly, despite excellent solubility of the complexes in $CDCl_3$, we could not observe the signals corresponding to **1**-**4** as described above. Comparison of the ^{1}H and ^{31}P NMR spectra recorded immediately after dissolution and 1 h later demonstrated the decomposition of the complex characterized by the appearance of additional signals and incorrect integration of the existing signals. Intrigued by the unusual instability of Au^{I} complexes in $CHCl_3$, we investigated the decomposition products of **2** arising from dissolution in chlorinated solvents.

Single crystal X-ray diffraction analysis revealed that **2** decomposed to form a coordination polymer comprising single stranded Au^{+}···Au^{+} filament bridged by diethyldithiocarbamate ligands. This type of polymers was previously prepared by the reaction of sodium diethyldithiocarbamate with $(CH_3)_2SAuCl$ or with PPh_3AuCl followed by precipitation of PPh_3 crystalls.[16, 21-24] We demonstrated that **2'** could also be obtained directly from **2** using chlorinated solvents. This unexpected transformation indicated the importance of careful solvent selection for the synthesis of Au^{I}-dithiocarbamate complexes and justified the use of pyridine for the preparation of **1**-**4**.

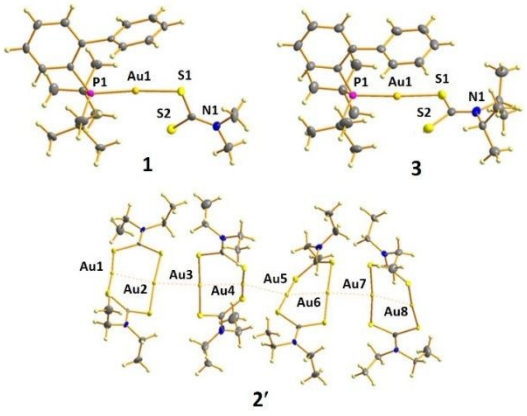

Fig. 1 Molecular structures of **1** (top, left), **3** (top, right) and Au^{+}···Au^{+} bonded Au^{I}-diethyldithiocarbamate polymer **2'** (bottom).

X-ray structure determination

The molecular structures of **1**, **3**, **4** and Au^{I} polymer **2'** were determined by solid-state X-ray diffraction analyses (Fig. 1 and S12), see Tables S2 and S3 for crystallographic data, bond lengths and bond angles). The coordination geometry around Au^{I} is distorted linear with S-Au-P bond angle of 174.99(3)°, 171.37(3)° and 172.967(18)° for **1**, **3** and **4**, respectively, typical for such type of Au(I)-phosphane complexes. The considerable deviation from linear was presumably due to the large steric encumbrance of the phosphane ligand, as well as the close intramolecular Au1…S2 contact of ≈3.035 Å. In general, the geometrical parameters of **1**, **3** and **4** were similar. The Au-S and Au-P bonds did not vary significantly and were *ca.* 2.26 Å and

ca. 2.32-2.34 Å, respectively, in agreement with the literature.[17, 25] The crystallographic parameters of Au polymer chain **2'** were also in good agreement with the literature.[24]

Electrochemical properties

Cyclic voltammograms of **2** and **4** were recorded in DMF/*n*-Bu_4NPF_6 using a conventional three-electrode configuration consisting of a glassy carbon working electrode, a platinum auxiliary electrodes and an Ag/AgCl/KCl reference electrode at potential scan rate of 100 mV/s (Fig. 2). The cyclic voltammogram of **2** demonstrated an irreversible oxidation at +0.67 V (vs. Ag/AgCl) or +0.86 V (vs. SHE). In general, the electrochemical behavior of **4** was identical to **2**, but E_a potential was slightly shifted to the more anodic region (+0.72 V vs. Ag/AgCl or +0.91 vs. SHE), which was consistent with the stronger electron-donating effect of the butyl group in the dithiocarbamate ligand. In the range from 0 to -2 V, no reduction processes for both complexes were detected. Similarly, an irreversible oxidation was previously reported for compounds [*t*-$Bu_3PAu(S_2CNMe_2)$] and [*t*-$Bu_3PAu(S_2CNEt_2)$],[17] as well as auranofin.[26]

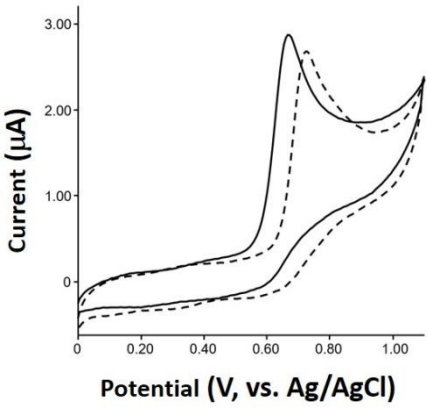

Fig. 2 Cyclic voltammogramms of compounds **2** (solid line) and **4** (dashed line) (*ca.* 10^{-3} M) in DMF in the range from 0 to 1.1 V at potential scan rate of 100 mV/s.

Inhibition of cancer cell viability

The *in vitro* anticancer activity of **1**-**4** and Au^I polymer **2'** was determined in human ovarian carcinoma cell line A2780 and its cDDP-resistant variant form A2780cis, as well as healthy embryonic kidney cells HEK293 (Table 3 and Fig. S13). All tested Au^I complexes demonstrated low micromolar to nanomolar toxicity, surpassing cDDP. Complex **2** exhibited the highest cytotoxicity and was 7× and 4× more cytotoxic than auranofin in A2780 and A2780cis, respectively. All Au^I complexes, including auranofin, exhibited lower resistance factor values compared to cDDP indicating their potential in treatment of cDDP-resistant tumors similar to Au^{III}-dithiocarbamate complexes.[18] Similarly, previously reported Au^I-dithiocarbamate complexes were equally potent in cDDP-sensitive and cDDP-resistant cell lines.[18] Only **4** demonstrated 3-fold selectivity towards cancer cells over healthy cells, indicating high toxicity of Au^I complexes, which could pose certain constraints for their future therapeutic development. It should be noted that polymeric Au chain was also cytotoxic against ovarian cancer cells, albeit less cytotoxic than monomer complexes **1**-**4**.

Table 1. Cytotoxicity of Au^I-phosphane complexes.

Entry	IC_{50}[a] (nM)			RF[b]	SF[c]	CA[d] (pmol/mg)
	A2780	A2780cis	HEK293			
1	51 ± 5	82 ± 31	74 ± 6	1.6	1.4	1053 ± 114
2	23 ± 2	38 ± 13	21 ± 7	1.7	0.9	3623 ± 1250
2'	243 ± 66	n.d.	312 ± 89	n.d.	1.3	n.d.
3	133 ± 29	145 ± 38	176 ± 20	1.1	1.3	998 ± 209
4	106 ± 7	190 ± 76	303 ± 39	1.8	2.9	1064 ± 245
cDDP	560 ± 140	5352 ± 1100	3966 ± 1151	9.6	7.1	n.d.

[a]Cytotoxicity given as 50% inhibitory concentrations (IC_{50}), determined by MTT assay with 72 h exposure; n.d. means not determined. Values are mean ± SEM from at least 3 independent expts. [b]Resistance Factor (RF) is determined as IC_{50}(A2780cis)/IC_{50}(A2780). [c]Selectivity Factor (SF) is determined as IC_{50}(HEK293)/IC_{50}(A2780). [d]Cellular accumulation (CA) in A2780 cells determined by ICP-MS after 24 h exposure to **1**-**4** (100 nM). Values are mean ± SEM obtained from at least 3 independent expts.

Cellular accumulation

The anticancer potential of cytotoxic substances depends on their ability to penetrate cellular membrane and accumulate in the intracellular space. Therefore, we determined the cellular accumulation of Au^I-phosphane complexes **1**-**4** and auranofin in A2780 cells after 24 h exposure (Table 3). Whereas complexes **1**, **3** and **4** demonstrated comparable cellular accumulation, the accumulation of **2** (3632 ± 1250 pmol Au/mg protein) was at least 3-fold higher than the accumulation of **1**, **3** and **4** and 1.5-fold higher than that of auranofin, in keeping with its highest cytotoxic activity.

Elucidation of mechanism of action

Induction of oxidative stress. Balanced control of reactive oxygen species (ROS) levels in cancer cells plays an important role in maintaining their high proliferation without damaging cellular components and functions. However, if the damage caused by excessive ROS levels cannot be managed, cell cycle arrest could eventually occur leading to cell death.[27] Cancer cells, having to cope with elevated ROS levels, are particularly sensitive to ROS insults. ROS-inducing agents take advantage of this limitation by directly or indirectly generating ROS within the cancer

intracellular environment. ROS-inducing properties of metal complexes, including auranofin, are well described.[8, 28-34] We therefore determined whether the cytotoxicity of the lead Au^{I}-phosphane complex **2** could be attributable to the generation of ROS. A2780 cells were incubated with **2** for 24 h in the absence or presence of the general antioxidant *N*-acetyl cysteine (NAC) and subsequently exposed to the ROS-sensitive fluorescent probe 2',7'-dichlorodihydro-fluorescein diacetate (H_2-DCFDA) (Fig. 3A). Fluorescence imaging demonstrated that ROS was observed only when cells were treated with **2** but not with the combination of **2** and NAC, suggesting its ability to elevate ROS levels in ovarian cancer cells.

Oxidative stress triggers cellular responses aimed to counteract ROS-induced damage. These responses are mediated by nuclear factor erythroid 2–related factor 2 (Nrf2) protein.[35] Hence, we determined the changes in Nrf2 expression upon 24 h treatment of A2780 cells with **2**. As expected, **2** caused dose-dependent increase of Nrf2 expression in line with the observed ROS induction (Fig. 3B). It was postulated that Au^{I} complexes do not directly generate ROS due to Au^{I}/Au^{III} cycling but rather as a consequence of sequestration of ROS responsive protein, e.g. thioredoxin reductase (TrxR).[36-45] This was supported by the oxidation potentials of **2** and **4**, as well as auranofin,[26] occurring outside biologically accessible redox potential window of -0.4V to +0.8V (vs SHE), suggesting indirect ROS induction.

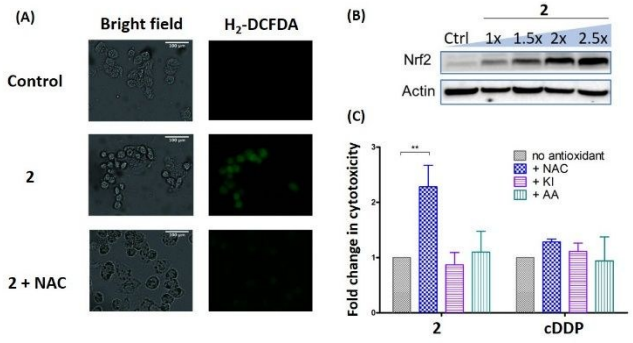

Fig. 3 Complex 2 induced oxidative stress in ovarian cells. (**A**) ROS detection by immunostaining. A2780 cells were incubated with **2** ($2.5\times IC_{50}$) for 24 h and subsequently stained with H_2-DCFDA (20 μM) for 15 min and visualized by fluorescent microscopy. The experiment with NAC was carried out similarly, but cells were additionally pre-treated with NAC (2 mM) for 1 h, followed by replacement of the fresh media without NAC and test compound. (**B**) Western blot analysis of Nrf2 protein. A2780 cells were treated with increasing concentrations of **2** (at concentrations corresponding to IC_{50} value from MTT experiment with exposure time of 24 h). (**C**) Fold change in cytotoxicity of **2** and cDDP upon 24 h co-incubation with various antioxidants (NAC (2 mM), KI (40 mM) and AA (acetic acid, 50 μM). Statistical analysis was performed by a one-way ANOVA using GraphPad Prism Software (GraphPad Software Inc., CA) with $p < 0.05$ considered as significant (** $p < 0.01$). Values are means ± standard errors of mean obtained from at least three independent biological experiments.

To determine the type of ROS that was induced by **2**, several antioxidants were pre-incubated with A2780 cells for 1 h before being exposed to **2** for 24 h. The residual cell viabilities of **2**-treated A2780 cells with or without antioxidant preincubation were quantified using MTT assay (Fig. 3C). The antioxidants used included general antioxidant *N*-acetylcysteine (NAC) which quenched HO·, HOCl and O_2^{-},[46, 47] ascorbic acid (AA) for O_2^{-},[48] and potassium iodide (KI) for $^1O_2$ (Fig. 3, S14 and Table S3).[49] Only pre-treatment with NAC significantly enhanced the survival of **2**-treated cells reflected by a 2.2-fold increase in IC_{50} values from 49.4 ± 15.9 nM without NAC to 113 ± 42 nM with NAC. KI and AA did not result in observable effects on the cell viability, thereby ruling out the induction of O_2^{-} and $^1O_2$. Since HOCl is not typically generated in non-phagocytic cells, the data suggested that cytotoxicity of **2** was dependent on the induction of hydroxyl radicals. In contrast, the effects of NAC on cDDP were not pronounced in agreement with its known ROS-independent mode of action.

Induction of ER stress. ER stress occurs upon increased levels of unfolded or misfolded proteins and results in an activation of pro-survival responses of cancer cells, such as unfolded protein response (UPR), aimed at restoring cellular homeostasis by putting a temporary halt to protein syntheses.[4, 6] The activation of UPR is reflected by the increased expression of GRP78 (or immunoglobulin heavy chain binding protein BiP), which is a major ER molecular chaperon, controlling the orchestration of ER stress sensors. When A2780 cells were treated with increasing concentrations of **2** for 24 h, the dose-dependent increase of BiP was observed, indicating cellular attempts to counteract the drug-induced damage (Fig. 4A). The pivotal role in the cytoprotective function of UPR is played by its PERK-eIF2α branch (PERK: (PKR)-like ER kinase (PERK), eIF2α: eukaryotic translation initiation factor).[50] During UPR, PERK undergoes trans-autophosphorylation leading to its activation and subsequently phosphorylates eIF2α, resulting in the general inhibition of protein translation and reduced protein load. Treatment of A2780 cells with **2** caused increased phosphorylation of PERK and eIF2α, characterized by the increased expression of p-PERK and p-eIF2α and decreased expression of native PERK in line with UPR activation (Fig. 4A).

Induction of p53-independent apoptosis and cell cycle arrest. When cellular attempts to counteract oxidative or ER stress-induced damage are no longer successful, CHOP-mediated pathways are activated to trigger apoptotic cell death to remove rogue cells.[7] Early apoptosis is characterized by the caspase-mediated cleavage of poly (ADP-ribose) polymerase (PARP). We therefore investigated whether **2** induced significant changes in CHOP and cleaved PARP expression levels. As expected, dose-dependent increase of CHOP expression and PARP cleavage was observed indicating the initiation of apoptotic processes (Fig. 4A and 4B). Other Au^{I} and Au^{III} complexes have also been shown to induce CHOP- and PARP-mediated apoptosis.[8, 9, 45, 51] Moreover, PARP1 zinc finger recognition domains were suggested as a selective target for some Au^{III} organometallics.[52] It is also known that one of the major mediators of apoptosis is the p53 protector gene, which is mutated in a large number of cancers, including high grade ovarian cancer.[53] Treatment of A2780 cells with **2** did not cause changes in p53 expression, suggesting p53-independent

apoptotic cell death, which is beneficial for treating cancers with the mutated p53 gene (Fig. 4B). Similarly, the comparison of cytotoxicity of Au^{III}-dithiocarbamate complexes in cell lines with different p53 status revealed that their anticancer properties were p53-independent.[18]

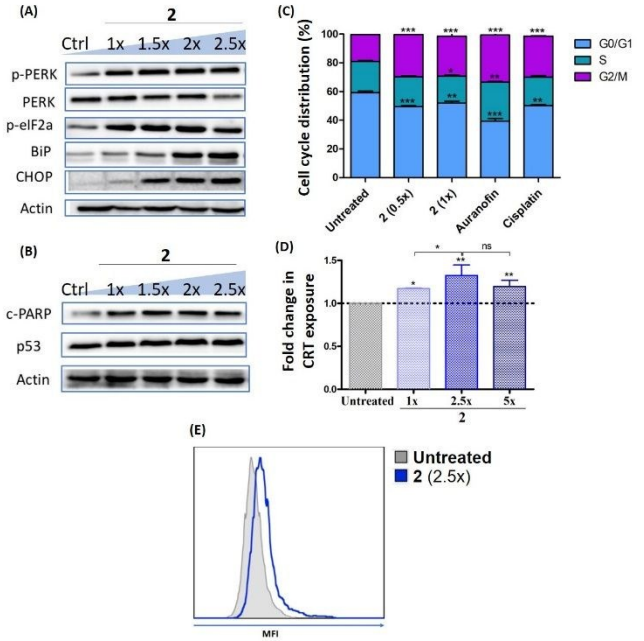

Fig. 4 Complex 2 induced ER stress-dependent responses in ovarian cancer cells. (**A**) Western blot analysis of ER stress proteins. (**B**) Western blot analysis of cleaved PARP and p53 proteins. (**A** and **B**) A2780 cells were treated with increasing concentrations of **2** (at concentrations corresponding to IC_{50} value from MTT experiment with exposure time of 24 h). (**C**) Flow cytometry analysis of cell cycle distribution in A2780 cells upon 24 h incubation with **2** (at concentrations corresponding to IC_{50} value from MTT experiment with exposure time of 24 h). (**D**) Fold change in CRT exposure upon 24 h incubation with **2** (at concentrations corresponding to IC_{50} value from MTT experiment with exposure time of 24 h) determined by flow cytometry. (**E**) Representative histogram showing the increase of mean fluorescence intensity (MFI) corresponding to CRT exposure upon 24 h incubation of A2780 cells with **2**. Statistical analysis was performed by a two-tailed t-test (**C**) or one-way ANOVA (**D**) using GraphPad Prism Software (GraphPad Software Inc., CA) with $p < 0.05$ considered as significant (* $p < 0.05$, ** $p < 0.01$, *** $p < 0.001$). Values are means ± standard errors of mean obtained from at least three independent biological expts.

The formation of cleaved PARP is associated with the DNA damage, which in turn affects cell cycle progression.[54] Since **2** induced PARP-mediated apoptosis, we expected that it would interfere with cancer cell cycle. Cell cycle analysis showed that **2** triggered cell cycle arrest at G_2/M phase when A2780 cells were treated with **2** at $1\times IC_{50}$, $2\times IC_{50}$ and $5\times IC_{50}$ for 24 h (Fig. 4C and S15). Similar patterns were observed when cells were treated with auranofin and cDDP, which is a DNA-alkylating agent.

Activation of CRT-mediated immune response. It is known that PERK-dependent eIF2α phosphorylation favors the translocation of CRT from the ER to the surface of the cell membrane.[55] The CRT exposure on the surface of severely stressed or dying cells plays a role of an "eat-me" signal and promote their engulfment by dendritic cells.[56] Since **2** demonstrated increased expression of both p-PERK and p-eIF2α in Western Blot experiments, we examined its effects on CRT exposure using flow cytometry. As expected, treatment of A2780 cells with **2** caused statistically significant increase in CRT-expressing cells similar to previously reported increase in CRT expression in auranofin-treated chronic lymphocytic leukemia cells (*ca.* 1.4-fold increase at IC_{50} concentration) (Fig. 4D).[8] It should be noted that incubation of ovarian cancer cells with **2** at $1\times IC_{50}$ and $2.5\times IC_{50}$ concentrations caused dose-dependent increase of CRT-expressing cells with no further increase at $5\times IC_{50}$. This could be related to the decrease of eIF2α phosphorylation commonly observed when the levels of ER stress become too severe. To conclude, **2** induced a dose-dependent CRT exposure which occurred as a consequence of PERK-mediated eIF2 phosphorylation and is therefore able to initiate the antigen presentation of cancer cells to lymphocytes and ignite subsequent anticancer immune responses.

Experimental Section

Materials and methods

All preparations were performed at r.t. All solvents were of analytical grade and used without further purification. Chloro[1,1′-biphenyl-2-yl)di-*tert*-butylphosphine]gold(I) was purchased from Strem Chemicals, Inc. Clinical-grade stable aqueous cDDP solution (1 mg/mL) was purchased from Hospira Pty Ltd (Melbourne, Australia). IGEPAL CA-630, DL-dithiothreitol (DTT), tetramethylethelenediamine, Tween-20, Ponceau S were purchased from Sigma-Aldrich (St Louis, MO, USA). RNase A was purchased from MP Biomedicals. Thiazolyl blue tetrazolium bromide (MTT) was purchased from Alfa Aesar, while Tris was purchased from Vivantis Technologies. Glycine, Hyclone Trypsin Protease 2.5% (10× solution), RPMI1640, fetal bovine serum (FBS), bovine serum albumin (BSA), Hank's Balanced Salt Solution (HBSS), Pierce Protease and Phosphatase Inhibitor Mini Tablets were purchased from Thermo Fisher Scientific. Hyclone Dulbecco's phosphate-buffered saline (10×, DPBS) was received from GE Healthcare Life Sciences. Biorad protein assay dye reagent concentrate, 30% acrylamide/bis solution, 5× Laemmli sample buffer and nitrocellulose membrane (0.2 μM) were purchased from Bio-Rad laboratories. Luminata Classico and Crescendo Western HRP substrate were purchased from Merck Millipore Corporation. Milli-Q grade water was obtained from a Milli-Q UV purification system (Sartorius Stedim Biotech S.A., Aubagne Cedex, France). All antibodies were from Cell Signaling Technologies (Beverly, MA, USA). Nitric acid (65 to 71%, TraceSELECT Ultra) for ICP-MS analysis was obtained from Fluka (Sigma Aldrich) and used without further purification. Au and Re standards for ICP-MS measurements were obtained from CPI International (Amsterdam, the Netherlands).

General procedure for the synthesis of 1-4

Equimolar amount of chloro[1,1′-biphenyl-2-yl)di-*tert*-butylphosphine]gold(I) was added dropwise to the solution of corresponding sodium dialkyldithiocarbamate in MeOH (20 mL) under inert atmosphere and the yellow reaction mixture was stirred for 30 min. After the addition of pyridine (30 mL) the solution became clear and was further stirred for 1 h, filtered and evaporated to dryness to yield the target complex. Crystals suitable for X-ray diffraction analysis were grown by slow diffusion of hexane into a CH_2Cl_2 solution.

1: Yield 85%. Elemental analysis (%) calcd for $C_{23}H_{33}AuNPS_2{\cdot}0.5CH_2Cl_2$ (658.05 g mol^{-1}): C 43.13, H 5.59, N 2.29; found: C 42.89, H 5.21, N 2.13%; IR cm^{-1}: 3056 (w), 2939 (w), 1580 (m), 1465 (s), 1440 (w), 1363 (s), 1251 (s), 1169 (m), 1123 (s), 1022 (m), 978 (s), 903 (w), 806 (m), 772 (m), 750 (s), 695 (s), 612 (s), 584 (m), 547 (s), 524 (s), 495(s); ^{1}H NMR (500.10 MHz, pyridine-d^5): δ = 1.39 (s, 9H, CH_3), 1.42 (s, 9H, CH_3), 3.44 (s, 6H, $N(CH_3)_2$), 7.25 (m, 1H, Ph), 7.33 (2H, Ph), 7.50 (m, 2H, Ph), 7.61 (m, 2H, Ph), 7.89 (m,

1H, Ph). ^{31}P NMR (202.44 MHz, pyridine-d^5): δ = 62.68 ppm (s, 1P); MS (ESI+): m/z 638.1 [M + Na]$^+$, 616.2 [M + H]$^+$; found: 638.1, 616.0. HR-MS (EI+): m/z 616.1530 [M + H]$^+$, found 616.1527.

2: Yield 78%. Elemental analysis (%) calcd for $C_{25}H_{37}AuNPS_2$ (643.18 g mol^{-1}): C, 46.64; H, 5.80; N, 2.18; found: C, 46.64; H, 5.72 ; N, 2.32; IR cm^{-1}: 3450 (br), 2031(w), 1629 (s), 1586 (m), 1506 (s), 1404 (m), 1369 (m), 1312 (s), 1202(m), 1117 (m), 1023 (m), 704 (w), 456(w); 1H NMR (500.10 MHz, pyridine-d5): δ = 1.24 (t, 6H, N(CH2CH3)2), 1.35 (s, 9H, CH3), 1.38 (s, 9H, CH3), 3.96 (q, 4H, N(CH_2CH_3)$_2$), 7.25 (m, 1H, Ph), 7.33 (m, 2H, Ph), 7.49 (m, 2H, Ph), 7.60 (m, 2H, Ph), 7.89 (m, 1H, Ph). ^{31}P NMR (202.44 MHz, pyridine-d^5): δ = 63.94 ppm (s, 1P); 1H NMR (500 MHz; DMSO-d^6): δ = 1.15 (t, 6H, N(CH_2CH_3)$_2$), 1.35 (s, 9H, CH_3), 1.39 (s, 9H, CH_3), 3.76 (q, 4H, N(CH_2CH_3)$_2$), 7.10 (m, 2H, Ph), 7.20 (m, 1H, Ph), 7.31 (m, 3H, Ph), 7.58 (m, 2H, Ph), 7.97 (m, 1H, Ph). MS (ESI+): m/z 666.6 [M + Na]$^+$, 644.6 [M + H]$^+$; found: 666.1, 644.0. HR-MS (EI+): m/z 644.1843 [M + H]$^+$, found 644.1849.

3: Yield 73%. Elemental analysis (%) calcd for $C_{27}H_{41}AuNPS_2 \cdot 0.25CH_2Cl_2$ (692.20 g mol^{-1}): C, 47.24; H, 6.04; N, 2.02; found: C, 47.40; H, 6.05; N, 1.97; IR cm^{-1}: 3056 (w), 2963 (m), 2863 (w), 1579 (m), 1468 (m), 1432 (m), 1384 (w), 1362 (s), 1296 (s), 1196 (m), 1172 (w), 1142 (s), 1036 (s), 938 (m), 902 (w), 846 (m), 807 (m), 775 (m), 749 (s), 698 (s), 611 (m), 584 (m), 524 (s), 475 (s), 443 (s), 438 (s), 431 (s); ^{1}H NMR (500.10 MHz, $CDCl_3$): δ = 1.42 (s, 9H, CH_3), 1.45 (s, 9H, CH_3), 1.52 (d, 12H, N($CH(CH_3)_2$)$_2$), 3.43 (sept, 2H, N($CH(CH_3)_2$)$_2$), 7.15 (m, 2H, Ph), 7.34 (m, 1H, Ph), 7.53 (m, 4H, Ph), 7.61 (m, 1H, Ph), 7.88 (m, 1H, Ph); 31P NMR (202.44 MHz, CDCl3): δ = 60.48 ppm (s, 1P); MS (ESI+): m/z 694.2 [M + Na]+; found: 694.1. HR-MS (EI+): m/z 672.2156 [M + H]+, found 672.2158.

4: Yield 69 %. Elemental analysis (%) calcd for $C_{29}H_{45}AuNPS_2$ (699.24 g mol^{-1}): C, 49.77; H, 6.49; N, 2.00; found: C, 49.54 ; H, 6.44 ; N, 2.24; IR cm^{-1}: 3061 (w), 2952 (w), 1934 (w), 1584 (w), 1493 (s), 1448 (s), 1424 (m), 1390 (s), 1359 (m), 1270 (s), 1204 (s), 1156 (w), 1123 (w), 1074 (m), 1025 (m), 985 (s), 936 (s), 881 (m), 807 (s), 771 (s), 749 (s), 726 (s), 697 (s), 632 (w), 586 (m), 550 (m), 521 (s) 494 (w), 472 (m); ^{1}H NMR (500 MHz; DMSO-d^6): δ = 0.86 (d, 12H, N($CH_2CH(CH_3)_2$)$_2$), 1.35 (s, 9H, CH_3), 1.36 (s, 9H, CH_3), 2.38 (sept, 2H, N($CH_2CH(CH_3)_2$)$_2$), 3.59 (d, 4H, N($CH_2CH(CH_3)_2$)$_2$), 7.10 (m, 2H, Ph), 7.20 (m, 1H, Ph), 7.29 (m, 3H, Ph), 7.58 (m, 2H, Ph), 7.98 (m, 1H, Ph); ^{1}H NMR (500 MHz; DMSO-d^6): δ = 0.86 (d, 12H, N($CH_2CH(CH_3)_2$)$_2$), 1.35 (s, 9H, CH3), 1.36 (s, 9H, CH3), 2.38 (sept, 2H, N(CH2CH(CH3)2)2), 3.59 (d, 4H, N($CH_2CH(CH_3)_2$)$_2$), 7.10 (m, 2H, Ph), 7.20 (m, 1H, Ph), 7.29 (m, 3H, Ph), 7.58 (m, 2H, Ph), 7.98 (m, 1H, Ph); ^{1}H NMR (500 MHz; methanol-d^4): δ = 1.00 (d, 6H, N($CH_2CH(CH_3)_2$)$_2$), 1.48-1.50 (m, 24H, CH_3 and N($CH_2CH(CH_3)_2$)$_2$), 2.36 (sept, 2H, N($CH_2CH(CH_3)_2$)$_2$), 3.89 (d, 4H, N($CH_2CH(CH_3)_2$)$_2$), 7.19 (m, 2H, Ph), 7.29 (m, 1H, Ph), 7.35 (m, 3H, Ph), 7.63 (m, 2H, Ph), 8.07 (m, 1H, Ph); ^{31}P NMR (202.44 MHz, methanol-d^4): δ = 64.05 ppm (s, 1P); HR-MS (EI+): m/z 700.2469 [M + H]$^+$, found 700.2467.

Instrumentation: ^{1}H and ^{31}P NMR spectra were recorded on a Varian Unity-500 MHz spectrometer equipped with a 5-mm switchable probe or a 5-mm inverse detection probe. Electrospray-ionization mass spectrometry (ESI-MS) spectra were obtained using a Thermo Finnigan MAT ESI-MS System. High-resolution electron-impact mass spectrometry (EI-MS) spectra were obtained using Agilent 7200 Q-TOF GCMS. ICP-OES determination of Au content and elemental analyses was performed in Chemical, Molecular and Analysis Centre, National University of Singapore with Optima ICP-OES (Perkin Elmer, Watham, MA, USA). The elemental analyses were carried out with a Perkin Elmer CHNS/O analyzer series II 2400. The absorbance of thiazolyl blue tetrazolium bromide (MTT) was measured by Synergy H1 hybrid multimode microplate reader (Bio-Tek, Winoosky, VT, USA). Au and Re contents in cells and tissues were determined by Agilent 7700 Series ICP-MS (Agilent Technologies, Santa Clara, CA, USA). Flow cytometry was performed on BD LSRFortessa Cell Analyzer (BD Biosciences, Franklin Lakes, NJ, USA). Fluorescent microscope images were collected through a laser scanning confocal microscope (Fluoview FV3000, Olympus). Western blot images were generated from G:Box (Syngene, Cambride, UK). Ultrapure water was purified by a Milli-Q UV purification system (Sartorius Stedim Biotech SA).

View Article Online
DOI: 10.1039/D0DT01411G

Cyclic voltammetry: The cyclic voltammograms (CV) were recorded with a 797 VA Computrace system (Metrohm, Switzerland). All measurements were performed with a conventional three-electrode configuration consisting of glassy carbon working and platinum auxiliary electrodes and an Ag/AgCl/KCl reference electrode. The solvent used in all experiments was DMF which was deoxygenated before use. Tetra-*n*-butylammonium hexafluorophosphate (0.1 M solution) was used as a supporting electrolyte. The concentration of the complexes was approximately 10^{-3} M. Ferrocene (Fc) was used as an internal standard, the Fc/Fc$^+$ potential was 0.43 V (vs. Ag/AgCl).

Single crystal X-ray diffraction studies: Single crystal X-ray diffraction was performed using either Bruker D8 Venture or Bruker SMART APEX X-ray diffractometer. Crystals were measured at low temperature (100 K) on a four circles goniometer using monochromatized Mo X-ray radiation (λ=0.71073 Å). Frames were integrated with the Bruker SAINT software package using a narrow-frame algorithm. Data were corrected for absorption effects using the multi-scan method implanted in the software (SADABS). Structure was solved using direct methods and subsequent differences Fourier maps, and then refined by least squares procedures on weighted F2 values using the SHELXL-version 2014/6 included in WinGX system programs for Windows. All non H-atoms were assigned anisotropic displacement parameters. H-atoms were located on difference Fourier maps then introduced as fixed contributors in idealized geometry with an isotropic thermal parameter fixed at 20% higher than those carbons atoms they were attached.

Cell lines and culture conditions: Human ovarian carcinoma cells A2780 and A2780cisR were obtained from ATCC. A2780 and A2780cisR cells were cultured in RPMI 1640 medium containing 10% fetal bovine serum (FBS) and 1% antibiotic-antimycotic (Gibco). CDDP at final concentration of 1 μM was added to A2780cis every three passages to maintain cDDP resistance. HEK293 were cultured in DMEM medium containing 10% FBS. Cells were grown in tissue culture 25 cm^2 flasks (BD Biosciences, Singapore) at 37°C in a humidified atmosphere of 95% air and 5% CO_2. The stock solutions of gold complexes were prepared in DMSO and the amount of gold was confirmed by ICP-OES. Clinical grade cDDP (1 mg/mL in aqueous buffer) was used and all dilutions were freshly prepared in respective growth media.

Cell culture and cytotoxicity assay (MTT assay): The cytotoxicity of the compounds was determined by colorimetric MTT [3-(4,5-dimethyl-2-thiazolyl)-2,5-diphenyl-2H tetrazolium bromide] assay. Cells were harvested from culture flasks by trypsinisation and seeded into Cellstar 96-well microculture plates (Greiner Bio-One) at the seeding density of 6000 cells per well (6×10^4 cells per mL). After the cells were allowed to resume exponential growth for 24 h, they were exposed to drugs at different concentrations in media for 72 h. The complexes were diluted in complete medium at the desired concentration and 100 μL of stock solutions were added to each well then serially diluted to other wells. After exposure for 72 h, cell media were replaced with 100 μL of MTT in media (5 mg/mL) and incubated for additional 60 min. Subsequently, the media were aspirated and the purple formazan crystals formed in viable cells were dissolved in DMSO (100 μL) per well. For cell viability assays involving inhibitors, cells were pretreated with NAC (2 mM), AA (50 μM) or KI (40 mM) for 1 h followed by replacement of the fresh media with indicated Au complex at desired concentrations for 24 h, similarly as described above. Optical densities were measured at 570 nm with a microplate reader. The quantity of viable cells was expressed in terms of treated/control (T/C) values by comparison to untreated control cells, and 50% inhibitory concentrations (IC_{50}) were calculated from concentration-effect curves by interpolation. Evaluation was based on means from at least three independent experiments, each comprising six replicates per concentration level.

Cellular accumulation: Cellular accumulation of Au compounds was determined in A2780 cells. Cells were seeded into Cellstar 6-well plates (Greiner Bio-one) at a density of 8.0×10^5 cells per mL (2 mL per well). After the cells were allowed to resume exponential growth for 24 h, they were exposed to gold complexes at different concentrations for 24 h. The cells were washed twice with 1 mL of PBS and lysed with lysis buffer [100 µL, 1% IGEPAL CA-630, 150 mM NaCl, 50 mM Tris-HCl (pH 8.0)] for 5–10 min at 4°C. The cell lysates were scraped from the wells and transferred to separate 1.5 mL microtubes. The supernatant was then collected after centrifugation (13000 rpm, 4°C for 15 min) and total protein content of each sample was quantified via Bradford's assay. Cell lysates were transferred to 2 mL glass vials and then digested with ultrapure 68% HNO_3 at 100°C for 24 h. The resulting solution was diluted to 2-4% v/v HNO_3 with ultrapure Milli-Q water and filtered. Au content of each sample was quantified by ICP-MS. Re was used as an internal standard. Au and Re were measured at m/z 197 and m/z 186, respectively. Metal standards for calibration curve (0, 0.5, 1, 2, 5, 10, 20, 40 ppb) were freshly prepared before each measurement. All readings were made in triplicates in He mode.

ROS detection using fluorescent microscopy: A2780 cells were seeded into Cellstar 6-well plates (Greiner Bio-one) with a cover slip at a density of 8.0×10^5 cells per mL (2 mL per well). Cells were allowed to resume exponential growth for 24 h before being exposed to **2** for 24 h. Wells were then washed with PBS twice before being incubated with H_2-DCFDA in colourless RPMI (2 mL, 20 µM) for 15 min in the darkness at 37°C. The cover slips were washed with PBS twice before being mounted on glass slides and the cells were visualized using fluorescence microscopy. For the experiment with NAC, cells were pretreated with NAC (2 mM) for 1 h followed by replacement of the fresh media with indicated Au complex at desired concentrations for 24 h.

Western Blot analysis: A2780 cells were seeded into Cellstar 6-well plates (Greiner Bio-one) at a density of 8.0×10^5 cells per mL (2 mL per well). After the cells were allowed to resume exponential growth for 24 h, they were exposed to **2** for 24 h. Subsequently, cells were washed with 1× PBS, scrapped using cell scraper and collected by centrifugation (450 × g, 1 min). Subsequently, cell pellets were lysed with cold lysis buffer (100 µL, 50 mM Tris pH 8.0, 150 mM NaCl, 1× protease and phosphatase inhibitor, 1% IGEPAL). After 20-30 min, the cells were centrifuged at 13000 g for 15 min at 4°C and total protein content of each sample was quantified via Bradford's assay. Equal quantities of protein (50 µg) were reconstituted in loading buffer (5% DDT, 5× Laemmli Buffer) and heated at 100°C for 10 min. The solutions were loaded onto a 10% SDS-PAGE and separated. Membrane transfer was carried out using nitrocellulose membranes (0.2 µm, Biorad). After blocking in 5% BSA in TBS-T (1× TBS with 0.1% Tween-20) for 1 h at r.t., the membrane was rinsed twice with TBS-T before incubating with primary antibodies (1:2500 dilution) for 12 h at 4°C. Membranes were washed 3 times with TBS-T, incubated with secondary antibodies (1:2500 dilution) for at least 1 h at r.t. and washed 3 times with wash buffer. Blots were incubated with Luminata Crescendo Western HRP substrate (Merck Millipore) and were imaged. The experiment was performed at least 3 times independently. List of primary antibodies used: NRF2 rabbit polyclonal IgG (sc-13032, Santa Cruz); CHOP rabbit mAb (5554S, Cell Signalling); BiP rabbit mAb (3177T, Cell Signalling); PERK rabbit mAb (5683T, Cell Signalling); p-eIFα rabbit mAb (5324, Cell Signalling); PARP rabbit mAb (9542, Cell Signalling); p53 rabbit polyclonal IgG (sc-6243, Santa Cruz); and Goat pAb to beta Actin (ab8229, Abcam). List of secondary antibodies used: Goat Anti-rabbit IgG (H+L) HRP (31460, Thermo Fisher Scientific) and Rabbit Anti-goat IgG (H+L) HRP (31402, Thermo Fisher Scientific).

Cell cycle analysis: A2780 cells were seeded into Cellstar 12-well plates (Greiner Bio-one) at a density of 2.0×10^5 cells per mL (1 mL per well). After the cells were allowed to resume exponential growth for 24 h, they were exposed to 2 for 24 h. The cells were harvested by trypsinization, washed twice with PBS and cell pellets were collected by centrifugation (450*g*, 1 min). The cells were fixed using chilled 70 % v/v EtOH/water (200 µL) on ice for 2 h. After the fixation, cells were washed with PBS (1x 200 µL) and resuspended in PI staining buffer (RNase A, 0.5 mg/mL and PI 40 µg/mL in PBS) for 1 h at 37ºC before analysis in a flow cytometer (BD LSR Fortessa).

Flow cytometric detection of CRT: A2780 cells were seeded into Cellstar 6-well plates (Greiner Bio-one) at a density of 8×10^5 cells per well. After the cells were allowed to resume exponential growth for 24 h, they were exposed to 2 for 24 h. Subsequently, cells were trypsinized using TrypLE™ Select Enzyme (1× in PBS), washed twice with PBS and cell pellets were collected by centrifugation (450*g*, 1 min). 1×10^6 cells was stained with mouse mAb against CRT [FMC 75] (Abcam) (1.5 µg in 50 µL of PBS) for 30 min in the dark at r.t. Cells were then washed thrice with 200 µL PBS (450*g*, 1 min), followed by the incubation with Alexa Fluor 488 anti-mouse IgG [RMG1-1] antibody (Biolegend) (1.5 µg in 50 µL of PBS) for 30 min in the dark at r.t. Subsequently, cells were washed thrice with PBS (450*g*, 1 min) and the pellets were resuspended in 7-AAD in PBS (1 µg/mL) and analyzed by flow cytometry.

Conclusions

In summary, we designed 4 Au^I-phosphane complexes with dialkyldithiocarbamate ligands and investigated their therapeutic potential for treatment of ovarian cancers. All complexes, as well as unexpectedly formed Au chain polymer demonstrated low micromolar to nanomolar cytotoxicity in both cDDP-sensitive and cDDP-resistant ovarian cancer cell lies. The highest cytotoxicity of the lead Au^I-diethyldithiocarbamate complex **2** was linked to its efficient cellular accumulation. The mechanism of action of **2** was based on the induction of integrative stress, including ROS insult, cell cycle interference and ER stress, leading to apoptosis. The activation of ER stress by **2** was followed by the CRT translocation to the cell membrane, which is associated with the activation of an immune system response.

Conflicts of interest

There are no conflicts to declare.

Acknowledgements

The authors would like to acknowledge the support by the Deanship of Scientific Research at King Fahd University of Petroleum and Minerals for funding this work through project No. SB 191032. Funding support from Ministry of Education of Singapore (R143-000-A66-112) is gratefully acknowledged.

Notes and references

1. R. Pokhriyal, R. Hariprasad, L. Kumar and G. Hariprasad, *Biomark. Cancer*, 2019, **11**, 1179299X19860815.
2. Y. Xu, C. Wang and Z. Li, *Mol. Clin. Oncol.*, 2014, **2**, 3-7.
3. S. Samanta, S. Tamura, L. Dubeau, P. Mhawech-Fauceglia, Y. Miyagi, H. Kato, R. Lieberman, R. J. Buckanovich, Y. G. Lin and N. Neamati, *Sci. Rep.*, 2020, **10**, 2160.
4. A. S. Lee and L. M. Hendershot, *Cancer Biol. Ther.*, 2006, **5**, 721-722.
5. J. R. Cubillos-Ruiz, S. E. Bettigole and L. H. Glimcher, *Cell*, 2017, **168**, 692-706.

6. B. Rah, D. Nayak, R. Rasool, S. Chakraborty, A. Katoch, H. Amin and A. Goswami, *Curr. Mol. Med.*, 2016, **16**, 690-701.
7. S. E. Logue, A. M. Gorman, P. Cleary, N. Keogh and A. Samali, *J. Carcinog. Mutagen.*, 2013, **S6**, DOI: 10.4172/2157-2518.s6-002.
8. W. Fiskus, N. Saba, M. Shen, M. Ghias, J. Liu, S. D. Gupta, L. Chauhan, R. Rao, S. Gunewardena, K. Schorno, C. P. Austin, K. Maddocks, J. Byrd, A. Melnick, P. Huang, A. Wiestner and K. N. Bhalla, *Cancer Res.* , 2014, **74**, 2520-2532.
9. J.-J. Zhang, R. W.-Y. Sun and C.-M. Che, *Chem. Commun.*, 2012, **48**, 3388-3390.
10. K.-B. Huang, F.-Y. Wang, X.-M. Tang, H.-W. Feng, Z.-F. Chen, Y.-C. Liu, Y.-N. Liu and H. Liang, *J. Med. Chem.*, 2018, **61**, 3478-3490.
11. T. Zou, C. T. Lum, C.-N. Lok, J.-J. Zhang and C.-M. Che, *Chem. Soc. Rev.*, 2015, **44**, 8786-8801.
12. A. Casini, R. W.-Y. Sun and I. Ott, *Met. Ions Life Sci.*, 2018, **18**, 199-218.
13. S. Jurgens, F. E. Kuhn and A. Casini, *Curr. Med. Chem.*, 2018, **25**, 437-461.
14. A. Jatoi and M. Clinic, Auranofin and Sirolimus in Treating Participants With Ovarian Cancer, https://clinicaltrials.gov/ct2/show/NCT03456700, (accessed April, 2020).
15. M. R. M. Williams, B. Bertrand, D. L. Hughes, Z. A. E. Waller, C. Schmidt, I. Ott, M. O'Connell, M. Searcey and M. Bochmann, *Metallomics*, 2018, **10**, 1655-1666.
16. A. A. A. Sulaiman, M. Altaf, A. A. Isab, A. Alawad, S. Altuwaijri and S. Ahmad, *Z. Anorg. Allg. Chem.*, 2016, **642**, 1454-1459.
17. M. Altaf, M. Monim-ul-Mehboob, A. A. A. Seliman, M. Sohail, M. I. M. Wazeer, A. A. Isab, L. Li, V. Dhuna, G. Bhatia and K. Dhuna, *Eur. J. Med. Chem.*, 2015, **95**, 464-472.
18. M. Altaf, M. Monim-ul-Mehboob, A.-N. Kawde, G. Corona, R. Larcher, M. Ogasawara, N. Casagrande, M. Celegato, C. Borghese, Z. H. Siddik, D. Aldinucci and A. A. Isab, *Oncotarget*, 2016, **8**.
19. R. Rubbiani, L. Salassa, A. de Almeida, A. Casini and I. Ott, *ChemMedChem*, 2014, **9**, 1205-1210.
20. V. Andermark, K. Goeke, M. Kokoschka, M. A. Abu el Maaty, C. T. Lum, T. Zou, R. W.-Y. Sun, E. Aguilo, L. Oehninger, L. Rodriguez, H. Bunjes, S. Woelfl, C.-M. Che and I. Ott, *J. Inorg. Biochem.*, 2016, **160**, 140-148.
21. D. Paliwoda, P. Wawrzyniak and A. Katrusiak, *J. Phys. Chem. Lett.*, 2014, **5**, 2182-2188.
22. D. D. Heinrich, J. C. Wang and J. P. Fackler, Jr., *Acta Crystallogr., Sect. C: Cryst. Struct. Commun.*, 1990, **C46**, 1444-1447.
23. F. Baril-Robert, M. A. Radtke and C. Reber, *J. Phys. Chem. C*, 2012, **116**, 2192-2197.
24. M. Hong, X. Lei, Z. Huang, B. Kang, F. Jiang and H. Liu, *Chin. Sci. Bull.*, 1993, **38**, 912-915.
25. S. Y. Ho and E. R. T. Tiekink, *Z. Kristallogr. NCS*, 2005, **220**, 362-364.
26. A. A. Mohamed, A. E. Bruce and M. R. M. Bruce, *Met.-Based Drugs*, 1999, **6**, 233-238.
27. A. Costa, A. Scholer-Dahirel and F. Mechta-Grigoriou, *Semin. Cancer Biol.*, 2014, **25**, 23-32.
28. U. Jungwirth, C. R. Kowol, B. K. Keppler, C. G. Hartinger, W. Berger and P. Heffeter, *Antioxid. Redox Signal.*, 2011, **15**, 1085-1127.
29. J. Yang, J.-X. Zhao, Q. Cao, L. Hao, D. Zhou, Z. Gan, L.-N. Ji and Z.-W. Mao, *ACS Appl. Mat. Interfaces*, 2017, **9**, 13900-13912.
30. J. Li, M. Tian, Z. Tian, S. Zhang, C. Yan, C. Shao and Z. Liu, *Inorg. Chem.*, 2018, **57**, 1705-1716.
31. M. Tian, J. Li, S. Zhang, L. Guo, X. He, D. Kong, H. Zhang and Z. Liu, *Chem. Commun.*, 2017, **53**, 12810-12813.
32. M.-H. Chen, F.-X. Wang, J.-J. Cao, C.-P. Tan, L.-N. Ji and Z.-W. Mao, *ACS Appl. Mat. Interfaces*, 2017, **9**, 13304-13314.
33. D. Y. Wong, W. W. Ong and W. H. Ang, *Angew. Chem. Int. Ed. Engl.*, 2015, **54**, 6483-6487.
34. S. Parveen, M. Hanif, E. Leung, K. K. H. Tong, A. Yang, J. Astin, G. H. De Zoysa, T. R. Steel, D. Goodman, S. Movassaghi, T. Söhnel, V. Sarojini, S. M. F. Jamieson and C. G. Hartinger, *Chem. Commun.*, 2019, **55**, 12016-12019.
35. M. B. Sporn and K. T. Liby, *Nat. Rev. Cancer*, 2012, **12**, 564-571.
36. C. Schmidt, L. Albrecht, S. Balasupramaniam, R. Misgeld, B. Karge, M. Broenstrup, A. Prokop, K. Baumann, S. Reichl and I. Ott, *Metallomics*, 2019, **11**, 533-545.
37. R. Rubbiani, E. Schuh, A. Meyer, J. Lemke, J. Wimberg, N. Metzler-Nolte, F. Meyer, F. Mohr and I. Ott, *MedChemComm*, 2013, **4**, 942-948.
38. A. Meyer, L. Oehninger, Y. Geldmacher, H. Alborzinia, S. Woelfl, W. S. Sheldrick and I. Ott, *ChemMedChem*, 2014, **9**, 1794-1800.
39. X. Cheng, P. Holenya, S. Can, H. Alborzinia, R. Rubbiani, I. Ott and S. Woelfl, *Mol. Cancer*, 2014, **13**, 221.
40. E. Vergara, A. Casini, F. Sorrentino, O. Zava, E. Cerrada, M. P. Rigobello, A. Bindoli, M. Laguna and P. J. Dyson, *ChemMedChem*, 2010, **5**, 96-102.
41. E. Schuh, C. Pfluger, A. Citta, A. Folda, M. P. Rigobello, A. Bindoli, A. Casini and F. Mohr, *J. Med. Chem.*, 2012, **55**, 5518-5528.
42. O. Karaca, V. Scalcon, S. M. Meier-Menches, R. Bonsignore, J. M. J. L. Brouwer, F. Tonolo, A. Folda, M. P. Rigobello, F. E. Kuehn and A. Casini, *Inorg. Chem.*, 2017, **56**, 14237-14250.
43. T. Zou, C. T. Lum, C.-N. Lok, W.-P. To, K.-H. Low and C.-M. Che, *Angew. Chem., Int. Ed.*, 2014, **53**, 5810-5814.
44. K. Yan, C.-N. Lok, K. Bierla and C.-M. Che, *Chem. Commun.* , 2010, **46**, 7691-7693.
45. R. W.-Y. Sun, C.-N. Lok, T. T.-H. Fong, C. K.-L. Li, Z. F. Yang, T. Zou, A. F.-M. Siu and C.-M. Che, *Chem. Sci.*, 2013, **4**, 1979-1988.
46. O. I. Aruoma, B. Halliwell, B. M. Hoey and J. Butler, *Free Radic. Biol. Med.*, 1989, **6**, 593-597.
47. M. Benrahmoune, P. Thérond and Z. Abedinzadeh, *Free Radic. Bio. Med.*, 2000, **29**, 775-782.
48. A. Nandi and I. B. Chatterjee, *J. Biosci.*, 1987, **11**, 435-441.
49. L. Huang, G. Szewczyk, T. Sarna and M. R. Hamblin, *ACS Infect. Dis.* , 2017, **3**, 320-328.
50. W. Rozpedek, D. Pytel, B. Mucha, H. Leszczynska, J. A. Diehl and I. Majsterek, *Curr. Mol. Med.*, 2016, **16**, 533-544.
51. S. K. Fung, T. Zou, B. Cao, P.-Y. Lee, Y. M. E. Fung, D. Hu, C.-N. Lok and C.-M. Che, *Angew. Chem., Int. Ed.*, 2017, **56**, 3892-3896.
52. M. N. Wenzel, S. M. Meier-Menches, T. L. Williams, E. Ramisch, G. Barone and A. Casini, *Chem. Commun.* , 2018, **54**, 611-614.
53. A. J. Cole, T. Dwight, A. J. Gill, K.-A. Dickson, Y. Zhu, A. Clarkson, G. B. Gard, J. Maidens, S. Valmadre, R. Clifton-Bligh and D. J. Marsh, *Sci. Rep.* , 2016, **6**, 26191.
54. C. Soldani and A. I. Scovassi, *Apoptosis*, 2002, **7**, 321-328.
55. T. Panaretakis, O. Kepp, U. Brockmeier, A. Tesniere, A.-C. Bjorklund, D. C. Chapman, M. Durchschlag, N. Joza, G. Pierron, P. van Endert, J. Yuan, L. Zitvogel, F. Madeo, D. B. Williams and G. Kroemer, *EMBO J.*, 2009, **28**, 578-590.
56. D. V. Krysko, K. S. Ravichandran and P. Vandenabeele, *Nat. Commun.*, 2018, **9**, 4644.

Table of Contents

View Article Online
DOI: 10.1039/D0DT01411G

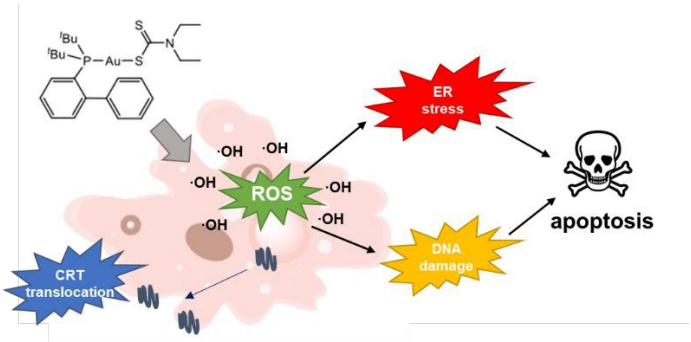

A series of highly cytotoxic Au^{I}-dithiocarbamate complexes was designed to counteract the pro-survival attempts of ovarian cancer cells by inducing severe integrative stress, including endoplasmic reticulum and oxidative stress, as well as cell cycle interference. As a result, drug treatment caused the surface exposure of calreticulin, which is a first step in the activation of immune system.